Control Engineering Practice 116 (2021) 104926

Contents lists available at ScienceDirect

Control Engineering Practice

journal homepage: www.elsevier.com/locate/conengprac

Geometric stochastic filter with guaranteed performance for autonomous navigation based on IMU and feature sensor fusion

Hashim A. Hashim [a,*], Mohammed Abouheaf [b], Mohammad A. Abido [c]

[a] Department of Engineering and Applied Science, Thompson Rivers University, Kamloops, British Columbia, Canada, V2C-0C8
[b] College of Technology, Architecture & Applied Engineering, Bowling Green State University, Bowling Green, 43402, OH, USA
[c] Electrical Engineering Department, King Fahd University of Petroleum and Minerals, Dhahran 31261, Saudi Arabia

ARTICLE INFO

Keywords:
Localization
Navigation
Position and orientation estimation
Stochastic systems
Stochastic differential equation
Gaussian noise
Sensor fusion

ABSTRACT

This paper concerns the estimation problem of attitude, position, and linear velocity of a rigid-body autonomously navigating with six degrees of freedom (6 DoF). The navigation dynamics are highly nonlinear and are modeled on the matrix Lie group of the extended Special Euclidean Group $\mathbb{SE}_2(3)$. A computationally cheap geometric nonlinear stochastic navigation filter is proposed on $\mathbb{SE}_2(3)$ with guaranteed transient and steady-state performance. The proposed filter operates based on a fusion of sensor measurements collected by a low-cost inertial measurement unit (IMU) and features (obtained by a vision unit). The closed loop error signals are guaranteed to be almost semi-globally uniformly ultimately bounded in the mean square from almost any initial condition. The equivalent quaternion representation is included in the Appendix. The filter is proposed in continuous form, and its discrete form is tested on a real-world dataset of measurements collected by a quadrotor navigating in three dimensional (3D) space.

1. Introduction

Robust and accurate navigation solutions for autonomous vehicles are essential (Barrau & Bonnabel, 2016; Buşoniu et al., 2020; Chebly, Talj, & Charara, 2019; Hashim & Eltoukhy, 2020; Hashim & Lewis, 2020; Hua, Manerikar, Hamel, & Samson, 2018). Indoor and outdoor applications, such as household cleaning devices, pipelines, terrain mapping, reef monitoring, exemplify situations when GPS might be unreliable and only low-cost measurement units (*e.g.*, inertial measurement unit (IMU)) might be available. In such a case GPS-independent navigation solutions are indispensable. A typical low-cost IMU module is composed of an accelerometer and a gyroscope which provide measurements of rigid-body's acceleration and angular velocity, respectively. In the absence of GPS, a cost-effective autonomous vehicle requires navigation solutions that rely on low-cost IMU and feature measurements collected by a vision unit. Consequently, linear velocity cannot be measured and its integration is impracticable due to the unbounded error growth resulting from sensor noise and bias (Woodman, 2007). Hence, autonomous navigation in space requires estimation of orientation (known as attitude), position, and linear velocity. Attitude can be successfully extracted given a low-cost IMU module using Gaussian filters (Choukroun, Bar-Itzhack, & Oshman, 2006; Markley, 2003; Zamani, Trumpf, & Mahony, 2013), nonlinear deterministic filters on the Special Orthogonal Group $\mathbb{SO}(3)$ (Batista, Silvestre, & Oliveira, 2012; Lee, 2012; Mahony, Hamel, & Pflimlin, 2008) or nonlinear stochastic filters on $\mathbb{SO}(3)$ (Hashim, 2020). The nonlinear deterministic filters in Baldwin, Mahony, and Trumpf (2009), Hashim, Brown, and McIsaac (2019), Lee (2012), Mahony et al. (2008) and Vasconcelos, Cunha, Silvestre, and Oliveira (2010) have been proven to be almost globally asymptotically stable, while nonlinear stochastic filters in Hashim (2020) are guaranteed to be almost globally asymptotically stable with a probability of one in mean square.

An inertial vision unit composed of a stereo vision unit and an IMU can be employed to extract rigid-body's pose - a combination of attitude and position. Pose estimation is commonly approached using Gaussian filters (Kalman-type filters) (Janabi-Sharifi & Marey, 2010). Nonetheless, nonlinear deterministic filters (Baldwin et al., 2009; Hua, Zamani, Trumpf, Mahony, & Hamel, 2011; Vasconcelos et al., 2010) and nonlinear stochastic filters (Hashim & Lewis, 2020) evolved on the Special Euclidean Group $\mathbb{SE}(3)$ have been deemed more suitable. Nonlinear deterministic pose filters have been shown to be almost globally asymptotically stable (Baldwin et al., 2009; Hashim et al., 2019; Vasconcelos et al., 2010), while nonlinear stochastic pose filters are guaranteed to be semi-globally uniformly ultimately bounded in mean square (Hashim & Lewis, 2020). It should be remarked that although the use of low-cost IMU and vision units facilitates the development of cost-effective autonomous vehicles, it requires robust solutions that accommodate for the measurement uncertainties.

The true six degrees of freedom (6 DoF) vehicle navigation dynamics are composed of attitude, position, and linear velocity dynamics

* Corresponding author.
E-mail address: h.a.hashiim@gmail.com (H.A. Hashim).

https://doi.org/10.1016/j.conengprac.2021.104926
Received 22 March 2021; Received in revised form 6 August 2021; Accepted 10 August 2021
Available online 26 August 2021

modeled on the Lie group of $\mathbb{SE}_2(3)$. The true dynamics are highly nonlinear, and are neither right nor left invariant. Navigation problem has been addressed using Kalman-type filters (KF) (Bijker & Steyn, 2008; Davari & Gholami, 2016), extended Kalman filters (EKF) (Anderson & Moore, 2012), unscented Kalman filters (UKF) (Zhang, Gu, Milios, & Huynh, 2005), multiplicative extended Kalman filter (MEKF) (Leishman & McLain, 2015), and particle filters (PFs) (Zhao, Skjetne, Blanke, & Dukan, 2014). However, the navigation solutions involving KF, EKF, UKF, MEKF, and PFs are not posed on $\mathbb{SE}_2(3)$. In view of the nonlinearity of the navigation dynamics, several solutions have been developed on the Lie group of $\mathbb{SE}_2(3)$, including invariant extended Kalman filter (IEKF) (Barrau & Bonnabel, 2016),a Riccati observer (Hua & Allibert, 2018), and a nonlinear stochastic observer (Hashim, 2021). Stochastic filters have been useful in several applications, for instance distributed delays (Wei, Li, & Stojanovic, 2021) and simultaneous localization and mapping (Hashim, 2021). The main shortcomings of these solutions are (1) the disregard for the IMU measurement noise and (2) the lack of transient and steady-state performance measures. Guaranteed convergence can be achieved by applying a prescribed performance function (PPF) (Bechlioulis & Rovithakis, 2008). PPF manipulates the error to initiate within a known large set and to decay systematically ultimately settling within a known small set (Bechlioulis & Rovithakis, 2008).

To summarize, the true navigation dynamics are (1) highly nonlinear, (2) posed on $\mathbb{SE}_2(3)$, and (3) reliant on angular velocity and acceleration. Addressing all of the above-mentioned navigation dynamics characteristics,

(1) this paper introduces a geometric nonlinear stochastic filter for inertial navigation posed on $\mathbb{SE}_2(3)$ reliant on measurements supplied by a typical low-cost IMU module, namely angular velocity and acceleration measurements commonly corrupted by noise,
(2) the proposed stochastic filter is characterized by guaranteed transient and steady-state performance of the attitude and position error,
(3) the closed loop error signals are shown to be almost semi-globally uniformly ultimately bounded in the mean square,
(4) although the stochastic filter is developed in a continuous form, its discrete representation is included, and
(5) the computational inexpensiveness of the proposed stochastic filter is demonstrated using a real-world three dimensional (3D) quadrotor dataset tested at a low sampling rate.

The proposed navigation filter is applicable to unmanned aerial vehicles as well as ground robots.

The paper is composed of seven sections: Section 2 presents important notation and preliminaries. Section 3 discusses the true navigation problem in a stochastic sense, available measurements, and error criteria. Section 4 reformulates the stochastic dynamics to follow systematic measures. Section 5 proposes a novel nonlinear stochastic filter. Section 6 reveals experimental results. Lastly, Section 7 concludes the work.

2. Preliminary material

A set of real numbers, nonnegative real numbers, and an n-by-m real dimensional space are defined by $\mathbb{R}$, $\mathbb{R}_+$, and $\mathbb{R}^{n\times m}$, respectively. The Euclidean norm of $x\in\mathbb{R}^n$ is $\|x\|=\sqrt{x^\top x}$, while the Frobenius norm of $M\in\mathbb{R}^{n\times m}$ is $\|M\|_F=\sqrt{\mathrm{Tr}\{MM^*\}}$ where $*$ denotes a conjugate transpose. $\mathbf{I}_n$ is an n-by-n identity matrix. For $M\in\mathbb{R}^{n\times n}$, the set of eigenvalues is $\lambda(M)=\{\lambda_1,\lambda_2,\dots,\lambda_n\}$ where $\overline{\lambda}_M=\overline{\lambda}(M)$ and $\underline{\lambda}_M=\underline{\lambda}(M)$ are the maximum and the minimum of $\lambda(M)$, respectively. $0_{n\times m}$ is a zero matrix and $1_{n\times m}$ is an n-by-m matrix of ones. $\mathbb{P}\{\cdot\}$ and $\mathbb{E}[\cdot]$ denote a probability and an expected value of a component, respectively. The fixed inertial- and body-frame are represented by $\{\mathcal{I}\}$ and $\{\mathcal{B}\}$, respectively. The vehicle's attitude is denoted by $R\in\mathbb{SO}(3)$ with $\mathbb{SO}(3)$ defined by

$$\mathbb{SO}(3)=\{R\in\mathbb{R}^{3\times3}|RR^\top=R^\top R=\mathbf{I}_3,\ \det(R)=+1\}$$

where $\det(\cdot)$ is a determinant. $\mathfrak{so}(3)$ is the Lie algebra of $\mathbb{SO}(3)$ given by

$$\mathfrak{so}(3)=\{[x]_\times\in\mathbb{R}^{3\times3}|[x]_\times^\top=-[x]_\times,x\in\mathbb{R}^3\}$$

where $[x]_\times$ is a skew symmetric matrix defined by

$$[x]_\times=\begin{bmatrix}0&-x_3&x_2\\x_3&0&-x_1\\-x_2&x_1&0\end{bmatrix}\in\mathfrak{so}(3),\quad x=\begin{bmatrix}x_1\\x_2\\x_3\end{bmatrix}$$

$\mathbf{vex}:\mathfrak{so}(3)\to\mathbb{R}^3$ describes the inverse mapping of $[\cdot]_\times$ such that $\mathbf{vex}([x]_\times)=x,\forall x\in\mathbb{R}^3$. $\mathcal{P}_a$ denotes the anti-symmetric projection on the $\mathfrak{so}(3)$ given by

$$\mathcal{P}_a(M)=\frac{1}{2}(M-M^\top)\in\mathfrak{so}(3),\forall M\in\mathbb{R}^{3\times3}$$

Let $\mathcal{Y}=\mathbf{vex}\circ\mathcal{P}_a$ denote the composition mapping such that

$$\mathcal{Y}(M)=\mathbf{vex}(\mathcal{P}_a(M))\in\mathbb{R}^3,\forall M\in\mathbb{R}^{3\times3}$$

Consider $\|R\|_{\mathrm{I}}$ as the Euclidean distance of $R\in\mathbb{SO}(3)$ expressed by

$$\|R\|_{\mathrm{I}}=\frac{1}{4}\mathrm{Tr}\{\mathbf{I}_3-R\}\in[0,1] \tag{1}$$

It is worth noting that $-1\le\mathrm{Tr}\{R\}\le3$ and $\|R\|_{\mathrm{I}}=\frac{1}{8}\|\mathbf{I}_3-R\|_F^2$, visit (Hashim, 2020). Let the attitude, position, and linear velocity of a vehicle navigating in 3D space be $R\in\mathbb{SO}(3)$, $P\in\mathbb{R}^3$, and $V\in\mathbb{R}^3$, respectively, for all $R\in\{\mathcal{B}\}$ and $P,V\in\{\mathcal{I}\}$. The Special Euclidean Group contains R and P defined by $\mathbb{SE}(3)=\mathbb{SO}(3)\times\mathbb{R}^3\subset\mathbb{R}^{4\times4}$, visit (Hashim & Lewis, 2020). The extended form of $\mathbb{SE}(3)$ is $\mathbb{SE}_2(3)=\mathbb{SO}(3)\times\mathbb{R}^3\times\mathbb{R}^3\subset\mathbb{R}^{5\times5}$ defined by

$$\mathbb{SE}_2(3)=\{X\in\mathbb{R}^{5\times5}\ |R\in\mathbb{SO}(3),P,V\in\mathbb{R}^3\} \tag{2}$$

$$X=\Psi(R,P,V)=\begin{bmatrix}R&P&V\\0_{1\times3}&1&0\\0_{1\times3}&0&1\end{bmatrix}\in\mathbb{SE}_2(3) \tag{3}$$

where $X\in\mathbb{SE}_2(3)$ is a homogeneous navigation matrix composed of rigid-body's attitude, position and linear velocity. Define $\mathcal{U}_m=\mathfrak{so}(3)\times\mathbb{R}^3\times\mathbb{R}^3\times\mathbb{R}\subset\mathbb{R}^{5\times5}$ as follows:

$$\mathcal{U}_m=\left\{u([\Omega]_\times,V,a,\kappa)\middle|\,[\Omega]_\times\in\mathfrak{so}(3),V,a\in\mathbb{R}^3,\kappa\in\mathbb{R}\right\}$$
$$u([\Omega]_\times,V,a,\kappa)=\begin{bmatrix}[\Omega]_\times&V&a\\0_{1\times3}&0&0\\0_{1\times3}&\kappa&0\end{bmatrix}\in\mathcal{U}_m\subset\mathbb{R}^{5\times5} \tag{4}$$

where $\Omega\in\mathbb{R}^3$, $V\in\mathbb{R}^3$, and $a\in\mathbb{R}^3$ denote the vehicle's true angular velocity, linear velocity, and apparent acceleration comprised of all non-gravitational forces affecting the vehicle, respectively, for all $\Omega,a\in\{\mathcal{B}\}$.

3. Problem formulation

From (3), the true dynamics of a rigid-body navigating in 3D space are given by

$$\begin{cases}\dot{R}&=R[\Omega]_\times\\\dot{P}&=V\\\dot{V}&=Ra+\vec{\mathrm{g}}\end{cases} \tag{5}$$

where $R\in\mathbb{SO}(3)$, $P\in\mathbb{R}^3$, and $V\in\mathbb{R}^3$ represent attitude, position, and linear velocity of a vehicle navigating in 3D space, respectively, and $\vec{\mathrm{g}}$ is a gravity vector. Also, $\Omega\in\mathbb{R}^3$ denotes the vehicle's true angular velocity, $V\in\mathbb{R}^3$ denotes the vehicle's true linear velocity, and $a\in\mathbb{R}^3$ denotes the apparent acceleration comprised of all non-gravitational forces affecting the vehicle. Note that $R,\Omega,a\in\{\mathcal{B}\}$ and $P,V\in\{\mathcal{I}\}$. Express (5) more compactly as

$$\dot{X}=XU-\mathcal{G}X \tag{6}$$

$$= \begin{bmatrix} R & P & V \\ 0_{1\times3} & 1 & 0 \\ 0_{1\times3} & 0 & 1 \end{bmatrix} \begin{bmatrix} [\Omega]_\times & 0_{3\times1} & a \\ 0_{1\times3} & 0 & 0 \\ 0_{1\times3} & 1 & 0 \end{bmatrix} - \begin{bmatrix} 0_{3\times3} & 0_{3\times1} & -\vec{g} \\ 0_{1\times3} & 0 & 0 \\ 0_{1\times3} & 1 & 0 \end{bmatrix} \begin{bmatrix} R & P & V \\ 0_{1\times3} & 1 & 0 \\ 0_{1\times3} & 0 & 1 \end{bmatrix}$$

where $X \in \mathbb{SE}_2(3)$, $U = u([\Omega]_\times, 0_{3\times1}, a, 1) \in \mathcal{U}_m$, and $\mathcal{G} = u(0_{3\times3}, 0_{3\times1}, -\vec{g}, 1) \in \mathcal{U}_m$, see (4). Note that $T_X\mathbb{SE}_2(3) \in \mathbb{R}^{5\times5}$ denotes the tangent space of $\mathbb{SE}_2(3)$ at point X where $\dot{X} : \mathbb{SE}_2(3) \times \mathcal{U}_m \to T_X\mathbb{SE}_2(3)$. When low-cost sensors are used in a GPS-denied environment, all the components of the navigation matrix X become unknown. Fig. 1 presents an ample illustration of the navigation problem.

The estimation can be performed using a set of sensor measurements. The measurements of Ω and a are as follows:

$$\begin{cases} \Omega_m &= \Omega + n_\Omega \in \mathbb{R}^3 \\ a_m &= a + n_a \in \mathbb{R}^3 \end{cases} \tag{7}$$

where n_Ω and n_a denote unknown bounded zero-mean noise contaminating Ω and a, respectively, and $\mathbb{E}[n_\Omega] = \mathbb{E}[n_a] = 0_{3\times1}$. Measurements of Ω and a can be easily obtained by a low-cost IMU module. Due to the fact that the derivative of a Gaussian process results in a Gaussian process, $n_\Omega = \mathcal{Q}d\beta_\Omega/dt$ and $n_a = \mathcal{Q}d\beta_a/dt$ as defined relative to the Brownian motion process vector (Jazwinski, 2007) where $\mathcal{Q} \in \mathbb{R}^{3\times3}$ is an unknown positive time-variant diagonal matrix. The covariance of n_Ω and n_a is $\mathcal{Q}^2 = \mathcal{Q}\mathcal{Q}^\top$. Note that the Brownian motion process is characterized by (Deng, Krstic, & Williams, 2001; Hashim, 2020; Ito & Rao, 1984; Jazwinski, 2007):

$$\begin{aligned} \mathbb{P}\{\beta_\Omega(0) = \beta_a(0) = 0\} &= 1 \\ \mathbb{E}[d\beta_\Omega/dt] = \mathbb{E}[d\beta_a/dt] &= 0_{3\times1} \\ \mathbb{E}[\beta_\Omega] = \mathbb{E}[\beta_a] &= 0_{3\times1} \end{aligned} \tag{8}$$

Thus, in the light of (1), the navigation dynamics in (5) can be expressed as a stochastic differential equation:

$$\begin{cases} d\|R\|_{\mathrm{I}} &= (1/2)\mathbf{vex}(\boldsymbol{\mathcal{P}}_a(R))^\top(\Omega_m dt - \mathcal{Q}d\beta_\Omega) \\ dP &= V dt \\ dV &= (Ra_m + \vec{g})dt - R\mathcal{Q}d\beta_a \end{cases} \tag{9}$$

where $dR = R[\Omega_m]_\times dt - R[\mathcal{Q}d\beta_\Omega]_\times$ and $\mathrm{Tr}\{R[\Omega_m]_\times\} = \mathrm{Tr}\{\boldsymbol{\mathcal{P}}_a(R)[\Omega_m]_\times\} = -2\mathbf{vex}(\boldsymbol{\mathcal{P}}_a(R))^\top\Omega_m$, visit (Hashim, 2020). To achieve adaptive stabilization, define

$$\sigma = [\sup_{t\geq0}\mathcal{Q}_{(1,1)}, \sup_{t\geq0}\mathcal{Q}_{(2,2)}, \sup_{t\geq0}\mathcal{Q}_{(3,3)}]^\top \tag{10}$$

Let n features be observed in the inertial-frame $p_i \in \{\mathcal{I}\}$ and measured in the body-frame such that

$$\begin{aligned} \overline{y}_i &= X^{-1}\overline{p}_i + [(n_i^y)^\top, 0, 0]^\top \in \mathbb{R}^5 \\ y_i &= R^\top(p_i - P) + n_i^y \in \mathbb{R}^3 \end{aligned} \tag{11}$$

with $X^{-1} = \begin{bmatrix} R^\top & -R^\top P & -R^\top V \\ 0_{1\times3} & 1 & 0 \\ 0_{1\times3} & 0 & 1 \end{bmatrix}$, $\overline{y}_i = [y_i^\top, 1, 0]^\top$, $\overline{p}_i = [p_i^\top, 1, 0]^\top$, and n_i^y being the noise associated with $y_i \in \{\mathcal{B}\}$.

Assumption 1. The number of noncollinear features available for measurement is greater than or equal to three in order to define a plane.

Definition 1 (*Ji & Xi, 2006*)**.** Consider the stochastic differential system in (9) with $x = [\|R\|_{\mathrm{I}}, P^\top, V^\top]^\top$. $x(t)$ is almost semi-globally uniformly ultimately bounded if for a known set $\Sigma \in \mathbb{R}^7$ and $x(t_0)$, there exist a constant $\kappa > 0$ and a time constant $\tau = \tau(\kappa, x(t_0))$ with $\mathbb{E}[\|x(t_0)\|] < \kappa, \forall t > t_0 + \tau$.

Definition 2. Translate the stochastic dynamics in (9) into a vector form such that

$$dx = f dt + h\overline{\mathcal{Q}}d\beta$$

with $x = [\|R\|_{\mathrm{I}}, P^\top, V^\top]^\top \in \mathbb{R}^7$, $f = [(1/2)\mathbf{vex}(\boldsymbol{\mathcal{P}}_a(R))^\top\Omega_m, V^\top, (Ra_m + \vec{g})^\top]^\top \in \mathbb{R}^7$, $h \in \mathbb{R}^{7\times9}$, $\overline{\mathcal{Q}} = \mathrm{diag}(\mathcal{Q}, \mathcal{Q}, \mathcal{Q}) \in \mathbb{R}^{9\times9}$, and $\beta = [\beta_\Omega^\top, 0_{3\times1}^\top, \beta_a^\top]^\top \in \mathbb{R}^9$. Let $\mathbb{V}(x)$ be a twice differentiable function $\mathbb{V}(x) \in C^2$. The differential operator $\mathcal{L}\mathbb{V}(x)$ is defined as follows:

$$\mathcal{L}\mathbb{V}(x) = \mathbb{V}_x^\top f + \frac{1}{2}\mathrm{Tr}\{h\overline{\mathcal{Q}}^2h^\top\mathbb{V}_{xx}\}$$

where $\mathbb{V}_x = \partial\mathbb{V}/\partial x$ and $\mathbb{V}_{xx} = \partial^2\mathbb{V}/\partial x^2$.

Lemma 1 (*Deng et al., 2001*)**.** *Let the stochastic system in (9) with $x = [\|R\|_{\mathrm{I}}, P^\top, V^\top]^\top$ be expressed as $dx = f dt + h\overline{\mathcal{Q}}d\beta$ with $f \in \mathbb{R}^7$, $h \in \mathbb{R}^{7\times9}$, $\overline{\mathcal{Q}} \in \mathbb{R}^{9\times9}$, and $\beta = [\beta_\Omega^\top, 0_{3\times1}^\top, \beta_a^\top]^\top \in \mathbb{R}^9$. Consider a twice differentiable potential function $\mathbb{V}(x)$ where $\mathbb{V} : \mathbb{R}^7 \to \mathbb{R}_+$. Let $\alpha_1(\cdot)$ and $\alpha_2(\cdot)$ be class $\mathcal{K}_\infty$ functions, and let constants $\eta_1 > 0$ and $\eta_2 \geq 0$ such that*

$$\alpha_1(x) \leq \mathbb{V}(x) \leq \alpha_2(x) \tag{12}$$

$$\begin{aligned} \mathcal{L}\mathbb{V}(x) &= (\partial\mathbb{V}/\partial x)^\top f + \frac{1}{2}\mathrm{Tr}\{h\overline{\mathcal{Q}}^2h^\top(\partial^2\mathbb{V}/\partial x^2)\} \\ &\leq -\eta_1\mathbb{V}(x) + \eta_2 \end{aligned} \tag{13}$$

Then for $x \in \mathbb{R}^7$, the stochastic dynamics in (9) have almost a unique strong solution on $[0, \infty)$. Also, the solution x is bounded in probability where

$$\mathbb{E}[\mathbb{V}(x)] \leq \mathbb{V}(x(0))\exp(-\eta_1 t) + \eta_2/\eta_1 \tag{14}$$

In addition, the inequality in (14) indicates that x is semi-globally uniformly ultimately bounded.

3.1. Estimates, error, and measurements setup

Define the estimate of $X \in \mathbb{SE}_2(3)$ in (3) as

$$\hat{X} = \Psi(\hat{R}, \hat{P}, \hat{V}) = \begin{bmatrix} \hat{R} & \hat{P} & \hat{V} \\ 0_{1\times3} & 1 & 0 \\ 0_{1\times3} & 0 & 1 \end{bmatrix} \in \mathbb{SE}_2(3) \tag{15}$$

with $\hat{R} \in \mathbb{SO}(3)$, $\hat{P} \in \mathbb{R}^3$, and $\hat{V} \in \mathbb{R}^3$ being the estimates of R, P, and V, respectively. Let the estimation error between X and $\hat{X}$ be

$$\tilde{X} = X\hat{X}^{-1} = \begin{bmatrix} \tilde{R} & \tilde{P} & \tilde{V} \\ 0_{1\times3} & 1 & 0 \\ 0_{1\times3} & 0 & 1 \end{bmatrix} \in \mathbb{SE}_2(3)$$

where $\hat{X}^{-1} = \Psi(\hat{R}^\top, -\hat{R}^\top\hat{P}, -\hat{R}^\top\hat{V})$, $\tilde{R} = R\hat{R}^\top$, $\tilde{P} = P - \tilde{R}\hat{P}$, and $\tilde{V} = V - \tilde{R}\hat{V}$. The navigation estimation problem aims to drive $X \to \hat{X}$ such that $\tilde{X} \to \mathbf{I}_5$, $\tilde{R} \to \mathbf{I}_3$, $\tilde{P} \to 0_{3\times1}$, and $\tilde{V} \to 0_{3\times1}$. Define the error

$$\begin{aligned} \overset{\circ}{y}_i &= \overline{p}_i - \tilde{X}^{-1}\overline{p}_i = \overline{p}_i - \hat{X}\overline{y}_i \\ &= [\underbrace{(p_i - \hat{R}y_i - \hat{P})}_{\tilde{p}_i - \tilde{P}}^\top, 0, 0]^\top \end{aligned} \tag{16}$$

where $\overset{\circ}{y}_i = [\tilde{y}_i^\top, 0, 0]^\top$, $\tilde{p}_i = \hat{p}_i - \tilde{R}p_i$, and $\tilde{P} = \hat{P} - \tilde{R}P$. Let $s_i > 0$ refer to the sensor confidence level of the ith feature. Define the following components with respect to the available vector measurements: $s_T = \sum_{i=1}^n s_i$, $p_c = \frac{1}{s_T}\sum_{i=1}^n s_i p_i$, $M = \sum_{i=1}^n s_i(p_i - p_c)(p_i - p_c)^\top$ such that $M = \sum_{i=1}^n s_i p_i p_i^\top - s_T p_c p_c^\top$, $\sum_{i=1}^n s_i(p_i - p_c)y_i^\top\hat{R}^\top = \sum_{i=1}^n s_i(p_i - p_c)(p_i - P)^\top\tilde{R} = M\tilde{R}$, and $\sum_{i=1}^n s_i\tilde{y}_i = \sum_{i=1}^n s_i(p_i - \hat{R}y_i - \hat{P}) = s_T\tilde{R}^\top\tilde{P}_\epsilon$ with $\tilde{P}_\epsilon = \tilde{P} - (\mathbf{I}_3 - \tilde{R})p_c$. It can be deduced that $\tilde{R} \to \mathbf{I}_3$ indicates that $\tilde{P}_\epsilon \to \tilde{P}$. Let us sum up the vector measurements:

$$\begin{cases} p_c &= \frac{1}{s_T}\sum_{i=1}^n s_i p_i, \quad s_T = \sum_{i=1}^n s_i \\ M &= \sum_{i=1}^n s_i p_i p_i^\top - s_T p_c p_c^\top \\ M\tilde{R} &= \sum_{i=1}^n s_i(p_i - p_c)y_i^\top\hat{R}^\top \\ \tilde{R}^\top\tilde{P}_\epsilon &= \frac{1}{s_T}\sum_{i=1}^n s_i(p_i - \hat{R}y_i - \hat{P}) \end{cases} \tag{17}$$

The vector measurements in (17) will be used to facilitate an explicit observer implementation.

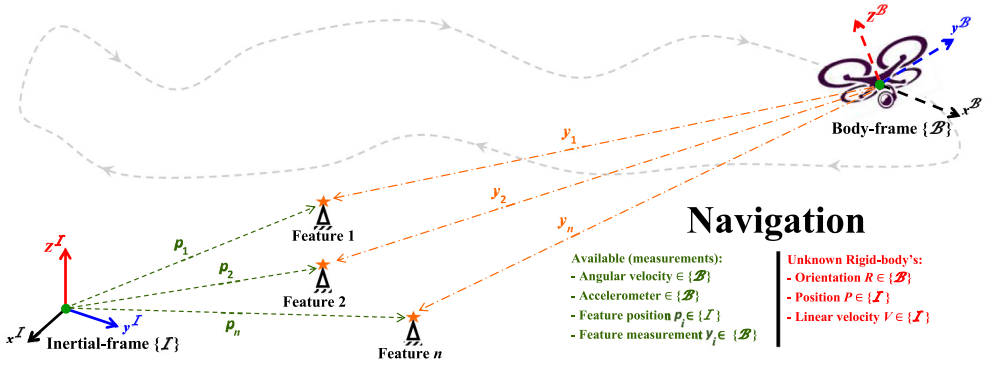

Fig. 1. Navigation estimation task.

Lemma 2. *Consider* $\tilde{R} \in \mathbb{SO}(3)$ *and* $M = M^\top \in \mathbb{R}^{3\times 3}$ *as in* (17). *Let* $\overline{\mathbf{M}} = \mathrm{Tr}\{M\}\mathbf{I}_3 - M$ *where* $\underline{\lambda}_{\overline{\mathbf{M}}}$ *and* $\overline{\lambda}_{\overline{\mathbf{M}}}$ *are the minimum and the maximum eigenvalues of* $\overline{\mathbf{M}}$, *respectively. For* $\|M\tilde{R}\|_{\mathrm{I}} = \frac{1}{4}\mathrm{Tr}\{M(\mathbf{I}_3 - \tilde{R})\}$ *and* $\boldsymbol{Y}(M\tilde{R}) = \mathbf{vex}(\mathcal{P}_a(M\tilde{R}))$,

$$\frac{\underline{\lambda}_{\overline{\mathbf{M}}}}{2}(1 + \mathrm{Tr}\{\tilde{R}\})\|M\tilde{R}\|_{\mathrm{I}} \leq \|\boldsymbol{Y}(M\tilde{R})\|^2 \tag{18}$$

$$2\overline{\lambda}_{\overline{\mathbf{M}}}\|M\tilde{R}\|_{\mathrm{I}} \geq \|\boldsymbol{Y}(M\tilde{R})\|^2 \tag{19}$$

Proof. See (Hashim (2020), Lemma 1). □

Let $\lambda(M) = \{\lambda_1, \lambda_2, \lambda_3\}$ where $\lambda_3 \geq \lambda_2 \geq \lambda_1$ and $\overline{\mathbf{M}} = \mathrm{Tr}\{M\}\mathbf{I}_3 - M$. Based on Assumption 1, a minimum of two eigenvalues of $\lambda(M)$ are greater than zero. Hence, (Bullo and Lewis (2004) page. 553): (1) $\overline{\mathbf{M}}$ is positive-definite, and (2) $\lambda(\overline{\mathbf{M}}) = \{\lambda_3 + \lambda_2, \lambda_3 + \lambda_1, \lambda_2 + \lambda_1\}$ with $\underline{\lambda}_{\overline{\mathbf{M}}} = \lambda_2 + \lambda_1 > 0$.

Definition 3 (*Hashim, 2020*)**.** Define the unstable set $\mathbb{U}_s \subset \mathbb{SO}(3)$ as

$$\mathbb{U}_s = \left\{ \tilde{R}(0) \in \mathbb{SO}(3) \middle| \, \mathrm{Tr}\{\tilde{R}(0)\} = -1 \right\} \tag{20}$$

where $\tilde{R}(0) \in \mathbb{U}_s$ if: $\tilde{R}(0) = \mathrm{diag}(1,-1,-1)$, $\tilde{R}(0) = \mathrm{diag}(-1,1,-1)$, or $\tilde{R}(0) = \mathrm{diag}(-1,-1,1)$. Based on (1), $\tilde{R}(0) \in \mathbb{U}_s$ indicates that $\|\tilde{R}(0)\|_{\mathrm{I}} = +1$.

4. Guaranteed performance

Define the error vector as follows:

$$e = [e_1, e_2, e_3, e_4]^\top = \left[\|M\tilde{R}\|_{\mathrm{I}}, \tilde{P}_\epsilon^\top \tilde{R}\right]^\top \in \mathbb{R}^4 \tag{21}$$

This section demonstrates how to guide the error e to reduce systematically and smoothly from a known large set to a known small set following the guaranteed measures of transient and steady-state performance. Hence, define the following prescribed performance function (PPF) (Bechlioulis & Rovithakis, 2008):

$$\xi_i(t) = (\xi_i^0 - \xi_i^\infty)\exp(-\ell_i t) + \xi_i^\infty, \quad \forall i = 1, 2, \ldots, 4 \tag{22}$$

where $\xi_i : \mathbb{R}_+ \to \mathbb{R}_+$, $\xi_i(0) = \xi_i^0 \in \mathbb{R}_+$ is the upper bound of the known large set, $\xi_i^\infty \in \mathbb{R}_+$ is the upper bound of the small set with $\lim_{t\to\infty} \xi_i(t) = \xi_i^\infty$, and $\ell_i > 0$ is the convergence rate of $\xi_i(t)$ from ξ_i^0 to ξ_i^∞ for all $i = 1, 2, 3, 4$. Define $e_i := e_i(t)$, $\xi_i := \xi_i(t)$, $\xi = [\xi_1, \ldots, \xi_4]^\top$, $\xi^0 = [\xi_1^0, \ldots, \xi_4^0]^\top$, $\xi^\infty = [\xi_1^\infty, \ldots, \xi_4^\infty]^\top$, and $\ell = [\ell_1, \ldots, \ell_4]^\top$ for all $\xi, \xi^0, \xi^\infty, \ell \in \mathbb{R}^4$. e_i follows the PPF in (22):

$$-\delta\xi_i < e_i < \xi_i, \text{ if } e_i(0) \geq 0 \tag{23}$$

$$-\xi_i < e_i < \delta\xi_i, \text{ if } e_i(0) < 0 \tag{24}$$

where $\delta \in [0, 1]$. Fig. 2 illustrates the concept of PPF for the two scenarios presented in (23) and (24).

Let e_i be defined as

$$e_i = \xi_i \mathcal{N}(E_i) \tag{25}$$

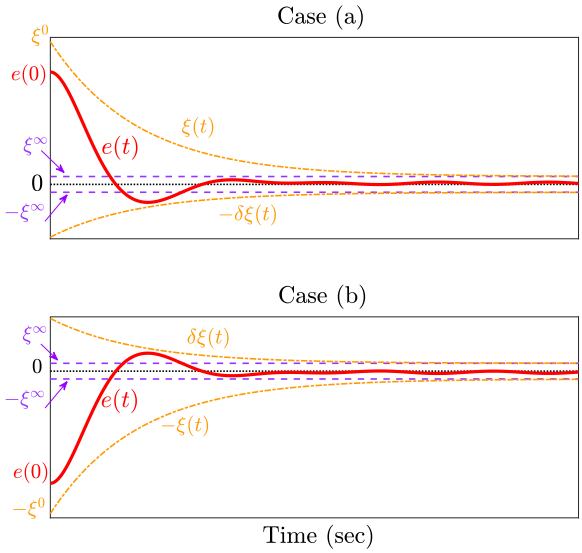

Fig. 2. Guaranteed performance of e_i in view of Case (a) Eq. (23); and Case (b) Eq. (24).

where $\mathcal{N}(E_i)$ is a smooth function and E_i is a transformed error (unconstrained error). To extract E_i, $\mathcal{N}(E_i)$ must follow Assumption 2:

Assumption 2 (*Bechlioulis & Rovithakis, 2008; Hashim et al., 2019; Hashim & Eltoukhy, 2020*)**.**

(1) $\mathcal{N}(E_i)$ is continuously differentiable and strictly increasing.

(2) $\mathcal{N}(E_i)$ is bounded such that

$$-\delta_i < \mathcal{N}(E_i) < \delta_i, \forall\, e_i(0) \in \mathbb{R}$$

where δ_i is a positive constant.

(3)

$$\lim_{E_i \to \pm\infty} \mathcal{N}(E_i) = \pm\delta_i, \forall\, e_i(0) \in \mathbb{R}$$

where δ_i is a positive constant.

The following function satisfies Assumption 2:

$$\mathcal{N}(E_i) = \frac{\delta_i \exp(E_i) - \delta_i \exp(-E_i)}{\exp(E_i) + \exp(-E_i)} \tag{26}$$

Define $\delta = [\delta_1, \delta_2, \delta_3, \delta_4]^\top$, $E = \left[E_R, E_P^\top\right]^\top$ for all $\delta, E \in \mathbb{R}^4$ where $E_R = E_1 \in \mathbb{R}$ and $E_P = [E_2, E_3, E_4]^\top \in \mathbb{R}^3$. The inverse transformation of (26) is $E_i = \mathcal{N}^{-1}(e_i/\xi_i)$ where

$$E_i = \frac{1}{2}\ln\frac{\delta_i + e_i/\xi_i}{\delta_i - e_i/\xi_i} \tag{27}$$

Remark 1 (Bechlioulis & Rovithakis, 2008; Hashim et al., 2019; Hashim & Eltoukhy, 2020)**.** Let the unconstrained error be as in (27). The transient and steady-state performance of e_i follow the PPF ξ_i, if and only if $E_i \in \mathcal{L}_\infty$.

Remark 2. Note that by definition $e_1 = \|M\tilde{R}\|_{\mathrm{I}} = \frac{1}{4}\mathrm{Tr}\{M(\mathbf{I}_3 - \tilde{R})\} \geq 0$ for all $\forall t \geq 0$. Also, $e_i \leq \xi_i$ indicates that $(\delta_i + e_i/\xi_i)/(\delta_i - e_i/\xi_i) \neq 1$ for all $e_i \neq 0$, and $(\delta_i + e_i/\xi_i)/(\delta_i - e_i/\xi_i) = 1$ if $e_i = 0$. Therefore, $E_i \neq 0 \forall e_i \neq 0$ and $E_i = 0$ if and only if $e_i = 0$.

Define

$$\Delta_i = \frac{1}{2\xi_i}\frac{\partial \mathcal{N}^{-1}\left(e_i/\xi_i\right)}{\partial\left(e_i/\xi_i\right)} = \frac{1}{2\xi_i}\left(\frac{1}{\delta_i + e_i/\xi_i} + \frac{1}{\delta_i - e_i/\xi_i}\right) \tag{28}$$

Therefore, the dynamics of $\dot{E}_i$ can be obtained as

$$\dot{E}_i = \Delta_i\left(\frac{d}{dt}e_i - \mu_i e_i\right) \tag{29}$$

Consider defining $\mu_R = \dot{\xi}_1/\xi_1$, $\mu_P = \mathrm{diag}(\dot{\xi}_2/\xi_2, \dot{\xi}_3/\xi_3, \dot{\xi}_4/\xi_4)$, $\Delta_R = \Delta_1$, and $\Delta_P = \mathrm{diag}(\Delta_2, \Delta_3, \Delta_4)$ for all $\mu_R, \Delta_R \in \mathbb{R}$ and $\mu_P, \Delta_P \in \mathbb{R}^{3\times 3}$.

5. Nonlinear stochastic navigation filter

This section pursues three main objectives: (1) providing a comprehensive discussion of a nonlinear stochastic complementary navigation filter evolved on $\mathbb{SE}_2(3)$, (2) constraining the error vector defined in (21) to behave following the predefined transient and steady state measures specified by the user, and (3) designing a robust filter that is able to produce accurate results irrespective of the noise level in measurements. The proposed filter can be utilized for unmanned aerial vehicles and ground robots. Let $\hat{\sigma}$ denote the estimate of σ defined in (10). Define the error between σ and $\hat{\sigma}$ as

$$\tilde{\sigma} = \sigma - \hat{\sigma} \in \mathbb{R}^3$$

Based on the set of measurements in (17), the error in (21), and the transformed error in (27), consider the following nonlinear stochastic navigation filter evolved directly on the Lie Group of $\mathbb{SE}_2(3)$:

$$\begin{aligned}\dot{\hat{X}} =& \hat{X}U_m - W\hat{X} \\ =& \begin{bmatrix}\hat{R} & \hat{P} & \hat{V}\\ 0_{1\times 3} & 1 & 0\\ 0_{1\times 3} & 0 & 1\end{bmatrix}\begin{bmatrix}[\Omega_m]_\times & 0_{3\times 1} & a_m\\ 0_{1\times 3} & 0 & 0\\ 0_{1\times 3} & 1 & 0\end{bmatrix} \\ & - \begin{bmatrix}[w_\Omega]_\times & w_V & w_a\\ 0_{1\times 3} & 0 & 0\\ 0_{1\times 3} & 1 & 0\end{bmatrix}\begin{bmatrix}\hat{R} & \hat{P} & \hat{V}\\ 0_{1\times 3} & 1 & 0\\ 0_{1\times 3} & 0 & 1\end{bmatrix}\end{aligned} \tag{30}$$

where $\hat{X} \in \mathbb{SE}_2(3)$, $U_m = u([\Omega_m]_\times, 0_{3\times 1}, a_m, 1) \in \mathcal{U}_m$ and $W = u([w_\Omega]_\times, w_V, w_a, 1) \in \mathcal{U}_m$. The equivalent detailed representation of (30) is as follows:

$$\begin{cases}\dot{\hat{R}} &= \hat{R}\,[\Omega]_\times - [w_\Omega]_\times \hat{R}\\ \dot{\hat{P}} &= \hat{V} - [w_\Omega]_\times \hat{P} - w_V\\ \dot{\hat{V}} &= \hat{R}a + \vec{g} - [w_\Omega]_\times \hat{V} - w_a\\ w_\Omega &= -k_w(\Delta_R E_R + 1)\boldsymbol{\Upsilon}(M\tilde{R})\\ &\quad -\frac{\Delta_R}{4}\frac{\|M\tilde{R}\|_{\mathrm{I}}+2}{\|M\tilde{R}\|_{\mathrm{I}}+1}\hat{R}\mathrm{diag}(\hat{R}^\top\boldsymbol{\Upsilon}(M\tilde{R}))\hat{\sigma}\\ w_V &= [p_c]_\times w_\Omega - \frac{k_v}{\epsilon}\Delta_P E_P - \ell_P \tilde{R}^\top\tilde{P}_\epsilon\\ w_a &= -\vec{g} - k_a\left(\frac{k_v}{\mu}\Delta_P + \mathbf{I}_3\right)\Delta_P E_P\\ k_R &= \gamma_\sigma\frac{\|M\tilde{R}\|_{\mathrm{I}}+2}{8}\Delta_R^2\exp(E_R)\\ \dot{\hat{\sigma}}_\Omega &= k_R\mathrm{diag}(\hat{R}^\top\boldsymbol{\Upsilon}(M\tilde{R}))\hat{R}^\top\boldsymbol{\Upsilon}(M\tilde{R}) - k_\sigma\gamma_\sigma\hat{\sigma}\end{cases} \tag{31}$$

where k_w, k_v, k_a, γ_σ, k_σ, μ, and ℓ_P are positive constants, $w_\Omega \in \mathbb{R}^3$, $w_V \in \mathbb{R}^3$, and $w_a \in \mathbb{R}^3$ are the correction factors $\forall\ w_\Omega, w_V, w_a \in \mathbb{R}^3$, $\boldsymbol{\Upsilon}(M\tilde{R}) = \mathbf{vex}(\boldsymbol{\mathcal{P}}_a(M\tilde{R}))$, $E_R = E_1$, and $E_P = [E_2, E_3, E_4]^\top$. Fig. 3 presents a block diagram of the observer proposed in (30) and detailed in (31).

Theorem 1. *Consider combining the stochastic dynamics in (9) with feature measurements ($\overline{y}_i = X^{-1}\overline{p}_i$) for all $i = 1, 2, \ldots, n$, angular velocity measurements ($\Omega_m = \Omega + n_\Omega$), and acceleration measurements ($a_m = a + n_a$). Suppose that Assumption 1 holds. Consider the nonlinear stochastic filter in (30) to be geared with $\overline{y}_i$, Ω_m, a_m, (17), (21), and (27) given that $E_R, E_P \in \mathcal{L}_\infty$ and $\tilde{R}(0) \notin \mathbb{U}_s$ as in (20). Then, (1) the error e in (21) is bounded by the dynamically reducing boundaries of ξ in (22) and (2) all the closed loop error signals are almost semi-globally uniformly ultimately bounded.*

Proof. Recall $\tilde{R} = R\hat{R}^\top$, $\tilde{P} = P - \tilde{R}\hat{P}$, $\tilde{P}_\epsilon = \tilde{P} - (\mathbf{I}_3 - \tilde{R})p_c$, and $\tilde{V} = V - \tilde{R}\hat{V}$. From (9) and (31), one has

$$\begin{cases}d\tilde{R} &= \tilde{R}[w_\Omega]_\times dt - \tilde{R}[\hat{R}Qd\beta_\Omega]_\times\\ d\tilde{P} &= (\tilde{V} + \tilde{R}w_V)dt + \tilde{R}[\hat{P}]_\times\hat{R}Qd\beta_\Omega\\ d\tilde{V} &= ((\mathbf{I}_3 - \tilde{R})g + \tilde{R}w_a)dt - \tilde{R}\hat{R}Qd\beta_a\\ &\quad -\tilde{R}[\hat{V}]_\times\hat{R}Qd\beta\end{cases} \tag{32}$$

With the objective of designing a filter that directly uses the measurements in (17), one finds

$$\begin{cases}d\|M\tilde{R}\|_{\mathrm{I}} &= \frac{1}{2}\boldsymbol{\Upsilon}(M\tilde{R})^\top w_\Omega dt - \frac{1}{2}\boldsymbol{\Upsilon}(M\tilde{R})^\top\hat{R}Qd\beta_\Omega\\ d\tilde{R}^\top\tilde{P}_\epsilon &= \underbrace{(\tilde{R}^\top\tilde{V} - [p_c - \tilde{R}^\top\tilde{P}_\epsilon]_\times w_\Omega + w_V)}_{f_P}dt\\ &\quad + \underbrace{-[\hat{P} - p_c + \tilde{R}^\top\tilde{P}_\epsilon]_\times\hat{R}}_{h_P}Qd\beta_\Omega\\ d\tilde{R}^\top\tilde{V} &= \underbrace{(-[w_\Omega]_\times\tilde{R}^\top\hat{V} + (\tilde{R} - \mathbf{I}_3)^\top\vec{g} + w_a)}_{f_V}dt\\ &\quad + \underbrace{-[[\tilde{R}^\top V]_\times\hat{R} \quad \hat{R}]}_{h_V}[Qd\beta_\Omega \quad Qd\beta_a]^\top\end{cases} \tag{33}$$

Therefore, from (33) and (29), one obtains the following stochastic dynamics:

$$\begin{cases}dE_R &= \Delta_R(d\|M\tilde{R}\|_{\mathrm{I}} - \mu_R\|M\tilde{R}\|_{\mathrm{I}}dt)\\ dE_P &= \underbrace{\Delta_P(f_P - \mu_P\tilde{R}^\top\tilde{P}_\epsilon)}_{\mathcal{F}_P}dt + \Delta_P h_P Qd\beta_\Omega\end{cases} \tag{34}$$

Consider the following Lyapunov function candidate $\mathbb{V} = \mathbb{V}(\|M\tilde{R}\|_{\mathrm{I}}, E_R, E_P, \tilde{R}^\top\tilde{V}, \tilde{\sigma})$:

$$\mathbb{V} = \mathbb{V}^a + \mathbb{V}^b \tag{35}$$

with $\mathbb{V}^a = \mathbb{V}^a(\|M\tilde{R}\|_{\mathrm{I}}, E_R, \tilde{\sigma})$ and $\mathbb{V}^b = \mathbb{V}^b(E_P, \tilde{R}^\top\tilde{V})$. The first part of (35) has the map $\mathbb{V}^a : \mathbb{SO}(3)\times\mathbb{R}\times\mathbb{R}^3 \to \mathbb{R}_+$ and is selected as

$$\mathbb{V}^a = \exp(E_R)\|M\tilde{R}\|_{\mathrm{I}} + \frac{1}{2\gamma_\sigma}\|\tilde{\sigma}\|^2 \tag{36}$$

where $E_R \geq 0$ and $\|M\tilde{R}\|_{\mathrm{I}} \geq 0 \forall t \geq 0$, $E_R \neq 0$ for all $\|M\tilde{R}\|_{\mathrm{I}} \neq 0$, and $E_R = 0$ only at $\|M\tilde{R}\|_{\mathrm{I}} = 0$ as discussed in Section 4. The first and the second partial derivatives of $\exp(E_R)\|M\tilde{R}\|_{\mathrm{I}}$ are $(\|M\tilde{R}\|_{\mathrm{I}} + 1)\exp(E_R)$ and $(\|M\tilde{R}\|_{\mathrm{I}} + 2)\exp(E_R)$, respectively. In view of (13), (33), and (34), one has

$$\begin{aligned}\mathcal{L}\mathbb{V}^a =& \exp(E_R)(\|M\tilde{R}\|_{\mathrm{I}} + 1)\Delta_R(\frac{1}{2}\boldsymbol{\Upsilon}(M\tilde{R})^\top w_\Omega - \mu_R\|M\tilde{R}\|_{\mathrm{I}})\\ &+ k_R\boldsymbol{\Upsilon}(M\tilde{R})^\top\hat{R}Q^2\hat{R}^\top\boldsymbol{\Upsilon}(M\tilde{R}) - \frac{1}{\gamma_\sigma}\tilde{\sigma}^\top\dot{\hat{\sigma}}\\ \leq& \exp(E_R)(\|M\tilde{R}\|_{\mathrm{I}} + 1)\Delta_R(\frac{1}{2}\boldsymbol{\Upsilon}(M\tilde{R})^\top w_\Omega - \mu_R\|M\tilde{R}\|_{\mathrm{I}})\\ &+ k_R\boldsymbol{\Upsilon}(M\tilde{R})^\top\hat{R}\mathrm{diag}(\sigma)\hat{R}^\top\boldsymbol{\Upsilon}(M\tilde{R}) - \frac{1}{\gamma_\sigma}\tilde{\sigma}^\top\dot{\hat{\sigma}}\end{aligned} \tag{37}$$

where Q^2 has been replaced by $\mathrm{diag}(\sigma)$ in (10). Replacing w_Ω and $\dot{\hat{\sigma}}$ with their definitions in (31) and recalling (18) in Lemma 2, one has

$$\begin{aligned}\mathcal{L}\mathbb{V}^a \leq& -(1 + \mathrm{Tr}\{\tilde{R}\})\frac{(k_w - c_m)\underline{\lambda}_{\overline{\mathbf{M}}}\Delta_R^2}{4}\exp(E_R)\|M\tilde{R}\|_{\mathrm{I}}\\ &+ k_\sigma\tilde{\sigma}^\top\hat{\sigma}\end{aligned} \tag{38}$$

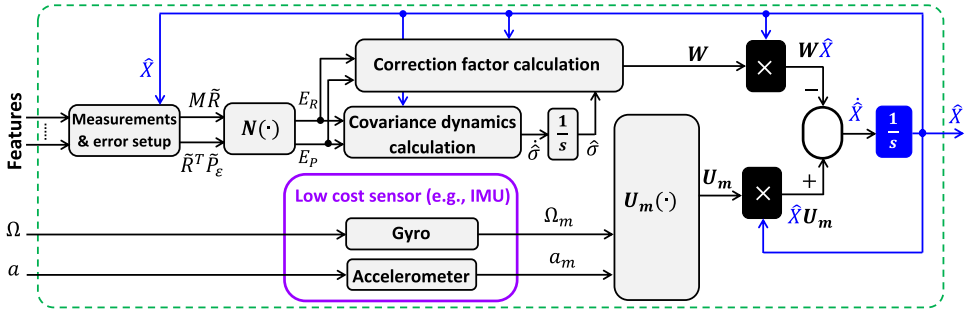

Fig. 3. Block diagram of the proposed nonlinear stochastic observer for inertial navigation.

Since $|\mu_R| \leq \ell_1$, let $c_m = \frac{4\ell_1}{\underline{\lambda}_{\mathbf{M}}(1+\mathrm{Tr}\{\tilde{R}\})}$ and select $k_w > c_m$. Also, in view of Young's inequality, one has $k_\sigma \tilde{\sigma}^\top \sigma \leq (k_\sigma/2)\|\sigma\|^2 + (k_\sigma/2)\|\tilde{\sigma}\|^2$. Define $c_R = \underline{\lambda}_{\mathbf{M}}(1+\mathrm{Tr}\{\tilde{R}\})$.

$$\mathcal{L}\mathbb{V}^a \leq -\frac{(k_w - c_m)c_R \Delta_R^2}{4}\exp(E_R)\|M\tilde{R}\|_{\mathrm{I}} - \frac{k_\sigma}{2}\|\tilde{\sigma}\|^2 + (k_\sigma/2)\|\sigma\|^2 \tag{39}$$

Turning our attention to the second part of (35), define the following Lyapunov function candidate:

$$\mathbb{V}^b = \frac{1}{4}\|E_P\|^4 + \frac{1}{4k_a}\|\tilde{R}^\top\tilde{V}\|^4 - \frac{1}{\mu}\|\tilde{R}^\top\tilde{V}\|^2\tilde{V}^\top\tilde{R}E_P \tag{40}$$

In view of (13), (33), and (34), one has

$$\begin{aligned}\mathcal{L}\mathbb{V}^b =& (\|E_P\|^2 E_P^\top - \frac{1}{\mu}\|\tilde{R}^\top\tilde{V}\|^2\tilde{V}^\top\tilde{R})\mathcal{F}_P \\ &+ (\frac{1}{k_a}\|\tilde{R}^\top\tilde{V}\|^2\tilde{V}^\top\tilde{R} - \frac{1}{\mu}\|\tilde{R}^\top\tilde{V}\|^2 E_P^\top)f_V \\ &+ \frac{1}{2}\mathrm{Tr}\left\{(\|E_P\|^2\mathbf{I}_3 + 2E_P E_P^\top)\Delta_P h_P \mathcal{Q}^2 h_P^\top \Delta_P\right\} \\ &+ \frac{1}{2k_a}\mathrm{Tr}\left\{(\|\tilde{R}^\top\tilde{V}\|^2\mathbf{I}_3 + 2E_P\tilde{V}^\top\tilde{R})h_V\mathcal{Q}^2 h_V^\top\right\}\end{aligned} \tag{41}$$

The equation in (41) can be presented in an inequality form as below:

$$\begin{aligned}\mathcal{L}\mathbb{V}^b \leq& -\underline{c}_2(\frac{4k_v - 3}{4})\|E_P\|^4 \\ &- (\frac{\underline{c}_1}{\mu} - \frac{\bar{c}_2}{2\mu k_v} - \frac{\|g\|}{2k_a} - \frac{\underline{c}_1}{4k_a})\|\tilde{R}^\top\tilde{V}\|^4 \\ &+ (\frac{\bar{c}_1 + \bar{c}_2}{\mu} + \frac{\underline{c}_1}{4k_a} + \frac{\|g\|\bar{\lambda}_M}{2\mu})\|\tilde{R}^\top\tilde{V}\|^2\|E_P\|^2 \\ &+ (\frac{\|g\|\bar{\lambda}_M}{2k_a} + \frac{\|g\|\bar{\lambda}_M}{2\mu})\|\tilde{R}^\top\tilde{V}\|^2\|\mathbf{I}_3 - \tilde{R}\|_F \\ &+ (\frac{3c_P}{2\underline{c}_2} + \frac{c_V}{4k_a\underline{c}_1})\|\sigma\|^2\end{aligned} \tag{42}$$

where $\underline{c}_1 = \min\{\Delta_P\}$, $\bar{c}_1 = \max\{\Delta_P\}$, $\underline{c}_2 = \min\{\Delta_P^2\}$, $\bar{c}_2 = \max\{\Delta_P^2\}$, $c_V = \sup_{t\geq 0}(1+\|V\|^2)$, and $c_P = \sup_{t\geq 0}\|P - p_c\|^2$. Let $c_x = \max\{\underline{c}_1, \bar{c}_1, \bar{c}_2, \|g\|\bar{\lambda}_M\}$ and $c_d = \max\{2\frac{\|g\|\bar{\lambda}_M}{\mu}, 2\frac{\|g\|\bar{\lambda}_M}{k_a}\}$. Consequently, one obtains

$$\begin{aligned}\mathcal{L}\mathbb{V}^b \leq& -\underline{c}_2(k_v - \frac{3}{4})\|E_P\|^4 - (\frac{\underline{c}_1}{\mu} - \frac{c_x}{k_a})\|\tilde{R}^\top\tilde{V}\|^4 \\ &+ \frac{5c_x}{4\mu}\|\tilde{R}^\top\tilde{V}\|^2\|E_P\|^2 + 2c_d\|\tilde{R}^\top\tilde{V}\|^2\|\mathbf{I}_3 - \tilde{R}\|_F \\ &+ (\frac{3c_P}{2\underline{c}_2} + \frac{c_V}{4k_a\underline{c}_1})\|\sigma\|^2\end{aligned} \tag{43}$$

such that

$$\begin{aligned}\mathcal{L}\mathbb{V}^b \leq& 2c_d\|\tilde{R}^\top\tilde{V}\|^2\|\mathbf{I}_3 - \tilde{R}\|_F + (\frac{3c_P}{2\underline{c}_2} + \frac{c_V}{4k_a\underline{c}_1})\|\sigma\|^2 \\ &- \varepsilon_{PV}^\top \underbrace{\begin{bmatrix} \underline{c}_2\frac{4k_v-3}{4} & \frac{5c_x}{8\mu} \\ \frac{5c_x}{8\mu} & \frac{\underline{c}_1}{\mu} - \frac{c_x}{k_v}\end{bmatrix}}_{A_1}\varepsilon_{PV}\end{aligned} \tag{44}$$

where $\varepsilon_{PV} = [\|E_P\|, \|\tilde{R}^\top\tilde{V}\|]^\top$. It can be deduced that A_1 can be made positive by selecting $k_v > \max\{3/4, \mu c_x/\underline{c}_1, c_x\mu^2/(\mu\underline{c}_1 - c_x)\}$. Recalling (35), (39), and (43), one obtains

$$\begin{aligned}\mathcal{L}\mathbb{V} \leq& -\frac{(k_w - c_m)c_R\Delta_R^2}{4}\exp(E_R)\|M\tilde{R}\|_{\mathrm{I}} - \underline{\lambda}_{A_1}\|\varepsilon_{PV}\|^2 \\ &+ 2c_d\|\tilde{R}^\top\tilde{V}\|^2\|\mathbf{I}_3 - \tilde{R}\|_F - \frac{k_\sigma}{2}\|\tilde{\sigma}\|^2 \\ &+ (\frac{k_\sigma}{2} + \frac{3c_P}{2\underline{c}_2} + \frac{c_V}{4k_a\underline{c}_1})\|\sigma\|^2\end{aligned} \tag{45}$$

which is

$$\begin{aligned}\mathcal{L}\mathbb{V} \leq& -\varepsilon_T^\top \underbrace{\begin{bmatrix} \frac{(k_w - c_m)c_R\underline{c}_2}{4} & c_d\mathbf{1}_{1\times 2} \\ c_d\mathbf{1}_{2\times 1} & \underline{\lambda}_1\mathbf{I}_2\end{bmatrix}}_{A_2}\varepsilon_T - \frac{k_\sigma}{2}\|\tilde{\sigma}\|^2 \\ &+ (\frac{3c_P}{2\underline{c}_2} + \frac{c_V}{4k_a\underline{c}_1} + \frac{k_\sigma}{2})\|\sigma\|^2 \\ \leq& -\underline{\lambda}_{A_2}\|\varepsilon_T\|^2 - \frac{k_\sigma}{2}\|\tilde{\sigma}\|^2 + \eta_2\|\sigma\|^2\end{aligned} \tag{46}$$

where $\varepsilon_T = [\sqrt{\exp(E_{\tilde{R}})\|M\tilde{R}\|_{\mathrm{I}}}, \|E_P\|^2, \|\tilde{R}^\top\tilde{V}\|^2]^\top$ and $\eta_2 = \frac{3c_P}{2\underline{c}_2} + \frac{c_V}{4k_a\underline{c}_1} + \frac{k_\sigma}{2}$. A_2 is made positive by selecting $(k_w - c_m)c_R\underline{c}_2\underline{\lambda}_1 > c_d^2$. Based on (46), one finds

$$\begin{aligned}\mathcal{L}\mathbb{V} \leq& -\underline{\lambda}_{A_2}(\exp(E_{\tilde{R}})\|M\tilde{R}\|_{\mathrm{I}} + \|E_P\|^4 + \|\tilde{R}^\top\tilde{V}\|^4) \\ &- \frac{k_\sigma}{2}\|\tilde{\sigma}\|^2 + \eta_2\|\sigma\|^2\end{aligned} \tag{47}$$

which means that

$$\frac{d\mathbb{E}[\mathbb{V}]}{dt} = \mathbb{E}[\mathcal{L}\mathbb{V}] \leq -\eta_1\mathbb{E}[\mathbb{V}] + \eta_2 \tag{48}$$

with $\eta_1 = \min\{\underline{\lambda}_{A_2}, k_\sigma/2\}$. In view of Lemma 1, the inequality in (48) shows that

$$0 \leq \mathbb{E}[\mathbb{V}(t)] \leq \mathbb{V}(0)\exp(-\eta_1 t) + \frac{\eta_2}{\eta_1},\ \forall t \geq 0.$$

Therefore, the vector $[\varepsilon_T^\top, \|\tilde{\sigma}\|]$ is almost semi-globally uniformly ultimately bounded which completes the proof. □

The filter in (31) is proposed in a continuous form. For the purposes of low-cost electronic kit implementation, a discrete version practicable at a low sampling rate is necessary. Let Δt denote a small sample time. The complete discreteimplementation steps are detailed in Algorithm 1. It should be noted that $\exp(\hat{U}_k\Delta t)$ and $\exp(-W_k\Delta t)$ denote exponential a matrix.

6. Experimental results

This section experimentally demonstrates the performance of the proposed nonlinear stochastic filter for inertial navigation with guaranteed performance on the Lie group of $\mathbb{SE}_2(3)$. The proposed stochastic filter in its discrete form (Algorithm 1) has been tested on the real-word data obtained from the EuRoC dataset (Burri et al., 2016). The

Algorithm 1 Discrete nonlinear stochastic filter with guaranteed performance

Initialization:

Set $\hat{R}[0] \in \mathbb{SO}(3)$, and $\hat{P}[0], \hat{V}[0], \hat{\sigma}[0] \in \mathbb{R}^3$

Start with $k = 0$ and select the design parameters

while (1) **do**

/* Prediction step */

$$\hat{X}_{k|k} = \begin{bmatrix} \hat{R}_{k|k} & \hat{P}_{k|k} & \hat{V}_{k|k} \\ 0_{1\times3} & 1 & 0 \\ 0_{1\times3} & 0 & 1 \end{bmatrix} \text{ and}$$

$\hat{U}_k = u([\Omega_m[k]]_\times, 0_{3\times1}, a_m[k], 1)$, see (4)

$\hat{X}_{k+1|k} = \hat{X}_{k|k} \exp(\hat{U}_k \Delta t)$

/* Update step */

$$\begin{cases} p_c & = \frac{1}{s_T}\sum_{i=1}^n s_i p_i[k], \quad s_T = \sum_{i=1}^n s_i \\ M_k & = \sum_{i=1}^n s_i p_i[k] p_i^\top[k] - s_T p_c p_c^\top \\ M\tilde{R}_k & = \sum_{i=1}^n s_i \left(p_i[k] - p_c\right) y_i^\top[k] \hat{R}_{k+1|k}^\top \\ \tilde{R}^\top \tilde{P}_\epsilon[k] & = \frac{1}{s_T}\sum_{i=1}^n s_i (p_i[k] - \hat{R}_{k+1|k} y_i[k] - \hat{P}_{k+1|k}) \end{cases}$$

$[e_1[k], e_2[k], e_3[k], e_4[k]]^\top = \left[||M\tilde{R}_k||_{\mathrm{I}}, \tilde{P}_\epsilon^\top \tilde{R}[k]\right]^\top$

for $i = 1:4$ /* Guaranteed Performance*/

$\xi_i[k] = (\xi_0 - \xi_\infty)\exp(-\ell k \Delta t) + \xi_\infty$

if $e_i[k] > \xi_i[k]$ **then**

$\xi_i[k] = e_i[k] + \epsilon$, /* ϵ is a small constant */

end if

$$\begin{cases} E_i & = \frac{1}{2}\ln\frac{\delta_i + e_i[k]/\xi_i[k]}{\delta_i - e_i[k]/\xi_i[k]} \\ \Delta_i & = \frac{1}{2\xi_i[k]}\left(\frac{1}{\delta_i + e_i[k]/\xi_i[k]} + \frac{1}{\delta_i - e_i[k]/\xi_i[k]}\right) \end{cases}$$

end for

Set $E_R[k] = E_1$, $E_P[k] = [E_2, E_3, E_4]^\top$, $\Delta_R[k] = \Delta_1$, and $\Delta_P[k] = \mathrm{diag}(\Delta_2, \Delta_3, \Delta_4)$.

$$\begin{cases} w_\Omega[k] & = -k_w(E_R[k] + 1)\Delta_R[k]\boldsymbol{Y}(M\tilde{R}_k) \\ & \quad - \frac{\Delta_R[k]}{4}\frac{||M\tilde{R}_k||_{\mathrm{I}}+2}{||M\tilde{R}_k||_{\mathrm{I}}+1}\hat{R}_k \mathrm{diag}(\hat{R}_k^\top \boldsymbol{Y}(M\tilde{R}_k))\hat{\sigma}_k \\ w_V[k] & = [p_c[k]]_\times w_\Omega[k] - \ell_P \tilde{R}^\top \tilde{P}_\epsilon[k] \\ & \quad - \frac{k_v}{\epsilon}\Delta_P[k]E_P[k] \\ w_a[k] & = -k_a\left(\frac{k_v}{\mu}\Delta_P[k] + \mathbf{I}_3\right)\Delta_P[k]E_P[k] \end{cases}$$

$W_k = u([w_\Omega[k]]_\times, w_V[k], w_a[k] - \vec{g}, 0)$, see (4)

$k_R = \gamma_\sigma \frac{||M\tilde{R}_k||_{\mathrm{I}}+2}{8}\Delta_R[k]^2 \exp(E_R[k])$

$\hat{\sigma}_{k+1} = \hat{\sigma}_k + \Delta t k_R \mathrm{diag}(\hat{R}_{k+1|k}^\top \boldsymbol{Y}(M\tilde{R}_k))\hat{R}_{k+1|k}^\top \boldsymbol{Y}(M\tilde{R}_k) - \Delta t k_\sigma \gamma_\sigma \hat{\sigma}_k$

$\hat{X}_{k+1|k+1} = \exp(-W_k \Delta t)\hat{X}_{k+1|k}$

$k = k + 1$

end while

dataset is comprised of the ground truth, IMU measurements provided by ADIS16448 at a sampling rate of 200 Hz, and stereo images collected by MT9V034 at a sampling rate of 20 Hz. The camera parameters were calibrated using the Stereo Camera Calibrator Application ensuring that the images are not distorted. Fig. 4 presents right and left feature detection. The detection of each photo in the EuRoC dataset (Burri et al., 2016) was tracked based on minimum eigenvalue feature detection using Kanade–Lucas–Tomasi (KLT) (Shi et al., 1994). The noise inherent to low-cost IMUs has been supplemented with additional noise of $n_\Omega = \mathcal{N}(0, 0.11)$ (rad/s) for the measurements of angular velocity while $n_a = \mathcal{N}(0, 0.1)$ (m/s^2) for the measurements of acceleration. Note that $\mathcal{N}(0, 0.11)$ is a notation of normally distributed noise with a zero mean and a standard deviation of 0.11. Owing to the lack of real-world features in the dataset, feature locations are selected arbitrarily. The maximum number of features were set to 30. The downloadable datasets can be accessed at the following URL. The initial covariance estimate is set to $\hat{\sigma}(0) = [0, 0, 0]^\top$, and the design parameters are selected as $k_w = 3$, $k_v = 3$, $k_a = 20$, $\gamma_\sigma = 3$, $k_\sigma = 0.1$, $\mu = 0.8$, $\epsilon = 0.8$,

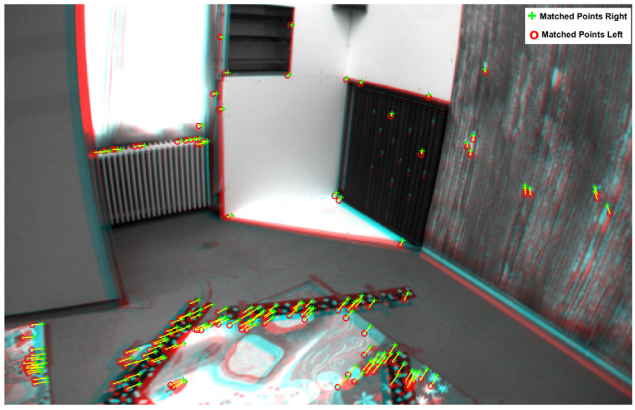

Fig. 4. Illustration of right and left feature detection. The detection tracking is performed using a stereo camera through the Computer Vision System Toolbox with MATLAB R2020a. The photo is part of the EuRoC dataset (Burri et al., 2016).

$\ell = [1, 1, 1, 1]^\top$, $\xi^\infty = [0.03, 0.1, 0.1, 0.1]^\top$, and

$$\xi_i^0 = \delta = \begin{bmatrix} 1.2\|M\tilde{R}(0)\|_{\mathrm{I}} + 0.5 \\ 2\tilde{R}(0)^\top \tilde{P}_\epsilon(0) + 2 \times 1_{3\times1} \end{bmatrix}$$

For large error in initialization, set the initial estimates of attitude, position, and linear velocity to

$$\hat{R}_0 = \hat{R}(0) = \mathbf{I}_3, \quad \hat{P}(0) = \hat{V}(0) = [0, 0, 0]^\top$$

The left portion of Fig. 5 illustrates rapid adaptation from large initial error in attitude and position and strong tracking capabilities of the filter to the true trajectory. The right portion of Fig. 5 reveals impressive convergence of the error components $\|R\hat{R}^\top\|_{\mathrm{I}}$, $\|P - \hat{P}\|$, and $\|V - \hat{V}\|$ from large initial error to the close neighborhood of the origin. Also, Fig. 5 confirms the robustness of the filter against the high levels of measurement noise. Fig. 6 shows remarkable tracking performance of the filter estimated orientation in terms of Euler angles ($\hat{\phi}$, $\hat{\theta}$, and $\hat{\psi}$) in comparison with the true vehicle's orientation (ϕ, θ, and ψ). Likewise, Fig. 7 illustrates impressive tracking performance of the filter estimated position ($\hat{x}$, $\hat{y}$, and $\hat{z}$) against the true vehicle's position (x, y, and z). To access experiment demonstration visit the Video Link. The real-world dataset experiment demonstrates the ability of the proposed stochastic filter to produce good results at low sampling rates and in presence of large initial error and measurement uncertainties. The performed testing indicates that the proposed filter is computationally cheap. As such, the proposed solution can be implemented using an inexpensive kit.

7. Conclusion

This paper addressed the problem of attitude, position, and linear velocity estimation of a rigid-body navigating with six degrees of freedom (6 DoF). A geometric nonlinear stochastic navigation filter on the matrix Lie group of $\mathbb{SE}_2(3)$ with guaranteed transient and steady-state performance has been proposed. The closed loop error signals have been shown to be almost semi-globally uniformly ultimately bounded in the mean square. The proposed filter produces good results given measurements supplied by low-cost inertial measurement and vision units. Experiments with real-world data obtained from quadrotor have demonstrated the strong tracking capabilities of the proposed filter as it rapidly and accurately estimates the unknown pose and linear velocity in presence of large initial attitude, position, and linear velocity error and high level of measurement uncertainties.

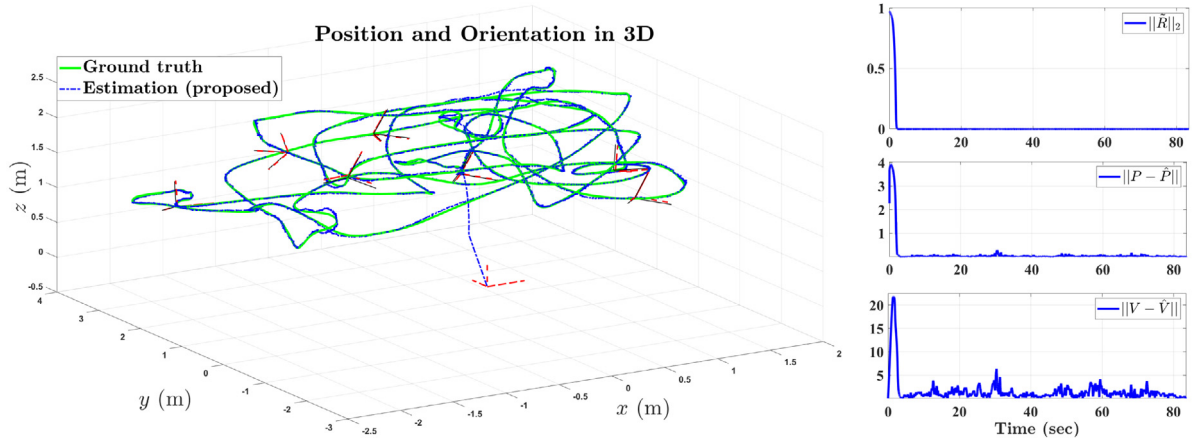

Fig. 5. Experimental validation using Vicon Room (V1_02_medium) dataset. In the left: the true vehicle trajectory (green solid-line) is plotted against the trajectory estimated by the proposed nonlinear stochastic discrete navigation filter (Algorithm 1; blue dashed-line). The true and the estimated final destinations are marked with a green circle and a blue star ⋆, respectively. Three axes illustrate the vehicle's true (black solid-line) and estimated (red dashed-line) attitude. On the right: the error components of attitude $\|R\hat{R}^\top\|_{\mathrm{I}}$, position $\|P-\hat{P}\|$, and velocity $\|V-\hat{V}\|$ are plotted in blue solid-line. To access experiment demonstration visit the Video Link. (For interpretation of the references to color in this figure legend, the reader is referred to the web version of this article.)

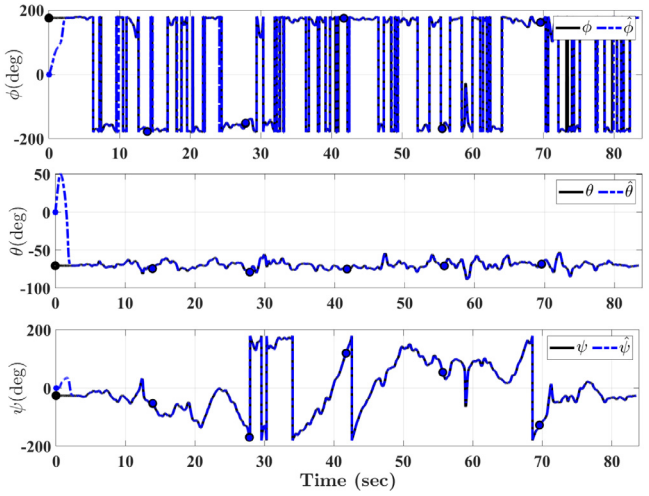

Fig. 6. Experimental validation using Vicon Room (V1_02_medium) dataset. Euler angles: True trajectory shown as a black solid line (ϕ, θ, and ψ) vs. estimated trajectory shown as a blue dashed-line ($\hat{\phi}$, $\hat{\theta}$, and $\hat{\psi}$). (For interpretation of the references to color in this figure legend, the reader is referred to the web version of this article.)

Declaration of competing interest

The authors declare that they have no known competing financial interests or personal relationships that could have appeared to influence the work reported in this paper.

Acknowledgments

This work was supported in part by Thompson Rivers University Internal research fund, Kamloops, British Columbia, Canada # 102315. The authors would like to thank **Maria Shaposhnikova** for proofreading the article.

Appendix. Quaternion of the proposed observers

Consider $Q = [q_0, q^\top]^\top \in \mathbb{S}^3$ as a unit-quaternion vector where $\mathbb{S}^3 = \{ Q \in \mathbb{R}^4 \,\big|\, \|Q\| = \sqrt{q_0^2 + q^\top q} = 1\}$ with $q_0 \in \mathbb{R}$ and $q \in \mathbb{R}^3$. Let $\hat{Q} \in \mathbb{S}^3$ be the estimate of $Q \in \mathbb{S}^3$ and consider the mapping from $\mathbb{S}^3$ to $\mathbb{SO}(3)$ to be $\mathcal{R}_{\hat{Q}} = (\hat{q}_0^2 - \|\hat{q}\|^2)\mathbf{I}_3 + 2\hat{q}\hat{q}^\top + 2\hat{q}_0\,[\hat{q}]_\times \in \mathbb{SO}(3)$. Recall the vector measurements in (17):

$$\begin{cases} p_c & = \frac{1}{s_T}\sum_{i=1}^n s_i p_i, \quad s_T = \sum_{i=1}^n s_i \\ M & = \sum_{i=1}^n s_i p_i p_i^\top - s_T p_c p_c^\top \\ M\tilde{R} & = \sum_{i=1}^n s_i (p_i - p_c) y_i^\top \mathcal{R}_{\hat{Q}}^\top \\ \tilde{R}^\top \tilde{P}_\varepsilon & = \frac{1}{s_T}\sum_{i=1}^n s_i (p_i - \mathcal{R}_{\hat{Q}} y_i - \hat{P}) \end{cases} \tag{49}$$

where $\boldsymbol{\Upsilon}(M\tilde{R}) = \mathbf{vex}(\boldsymbol{\mathcal{P}}_a(M\tilde{R}))$ and $\|M\tilde{R}\|_{\mathrm{I}} = \frac{1}{4}\mathrm{Tr}\{M(\mathbf{I}_3 - \tilde{R})\}$. Define $[e_1, e_2, e_3, e_4]^\top = \left[\|M\tilde{R}\|_{\mathrm{I}}, \tilde{P}_\varepsilon^\top \tilde{R}\right]^\top$ such that

$$\begin{cases} E_i & = \frac{1}{2}\ln\frac{\delta_i + e_i[k]/\xi_i[k]}{\delta_i - e_i[k]/\xi_i[k]} \\ \Delta_i & = \frac{1}{2\xi_i[k]}\left(\frac{1}{\delta_i + e_i[k]/\xi_i[k]} + \frac{1}{\delta_i - e_i[k]/\xi_i[k]}\right) \end{cases} \tag{50}$$

for all $i = 1, \ldots, 4$. Let $E = \left[E_R, E_P^\top\right]^\top$, $\Delta_R = \Delta_1$, and $\Delta_P = \mathrm{diag}(\Delta_2, \Delta_3, \Delta_4)$. The equivalent quaternion-based navigation filter in (31) is given below:

$$\begin{cases} \Theta_m = \begin{bmatrix} 0 & -\Omega_m^\top \\ \Omega_m & -[\Omega_m]_\times \end{bmatrix}, \quad \Psi = \begin{bmatrix} 0 & -w_\Omega^\top \\ w_\Omega & [w_\Omega]_\times \end{bmatrix} \\ \dot{\hat{Q}} = \frac{1}{2}\Theta_m \hat{Q} - \frac{1}{2}\Psi\hat{Q} \\ \dot{\hat{P}} = \hat{V} - \left[w_\Omega\right]_\times \hat{P} - w_V \\ \dot{\hat{V}} = \mathcal{R}_{\hat{Q}} a_m + \vec{\mathrm{g}} - \left[w_\Omega\right]_\times \hat{V} - w_a \\ w_\Omega = -k_w(\Delta_R E_R + 1)\boldsymbol{\Upsilon}(M\tilde{R}) \\ \qquad - \frac{\Delta_R}{4}\frac{\|M\tilde{R}\|_{\mathrm{I}}+2}{\|M\tilde{R}\|_{\mathrm{I}}+1}\hat{R}\mathrm{diag}(\hat{R}^\top \boldsymbol{\Upsilon}(M\tilde{R}))\hat{\sigma} \\ w_V = \left[p_c\right]_\times w_\Omega - \frac{k_v}{\varepsilon}\Delta_P E_P - \ell_P \tilde{R}^\top \tilde{P}_\varepsilon \\ w_a = -\vec{\mathrm{g}} - k_a\left(\frac{k_v}{\mu}\Delta_P + \mathbf{I}_3\right)\Delta_P E_P \\ k_R = \gamma_\sigma \frac{\|M\tilde{R}\|_{\mathrm{I}}+2}{8}\Delta_R^2 \exp(E_R) \\ \dot{\hat{\sigma}}_\Omega = k_R \mathrm{diag}(\hat{R}^\top \boldsymbol{\Upsilon}(M\tilde{R}))\hat{R}^\top \boldsymbol{\Upsilon}(M\tilde{R}) - k_\sigma \gamma_\sigma \hat{\sigma} \end{cases} \tag{51}$$

Appendix B. Supplementary data

Supplementary material related to this article can be found online at https://doi.org/10.1016/j.conengprac.2021.104926.

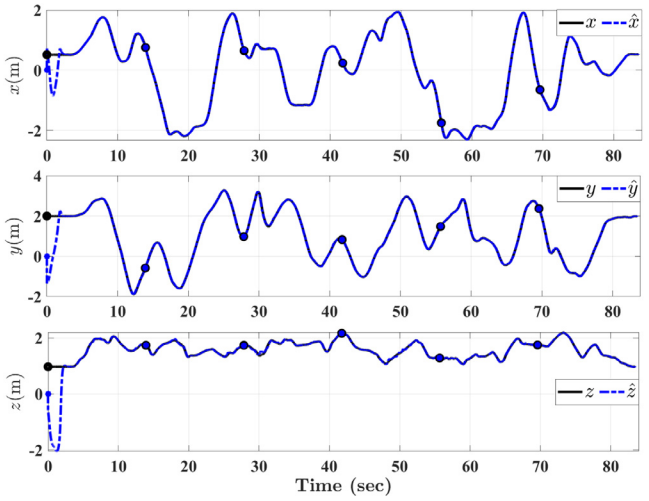

Fig. 7. Experimental validation using Vicon Room (V1_02_medium) dataset. Position in 3D space: True trajectory shown as a black solid line (x, y, and z) vs. estimated trajectory shown as a blue dashed-line ($\hat{x}$, $\hat{y}$, and $\hat{z}$). (For interpretation of the references to color in this figure legend, the reader is referred to the web version of this article.)

References

Anderson, B. D., & Moore, J. B. (2012). *Optimal Filtering*. Courier Corporation.

Baldwin, G., Mahony, R., & Trumpf, J. (2009). A nonlinear observer for 6 dof pose estimation from inertial and bearing measurements. In *Robotics and Automation, 2009. ICRA'09. IEEE International Conference on* (pp. 2237–2242). IEEE.

Barrau, A., & Bonnabel, S. (2016). The invariant extended kalman filter as a stable observer. *IEEE Transactions on Automatic Control*, *62*(4), 1797–1812.

Batista, P., Silvestre, C., & Oliveira, P. (2012). Globally exponentially stable cascade observers for attitude estimation. *Control Engineering Practice*, *20*(2), 148–155.

Bechlioulis, C. P., & Rovithakis, G. A. (2008). Robust adaptive control of feedback linearizable mimo nonlinear systems with prescribed performance. *IEEE Transactions on Automatic Control*, *53*(9), 2090–2099.

Bijker, J., & Steyn, W. (2008). Kalman filter configurations for a low-cost loosely integrated inertial navigation system on an airship. *Control Engineering Practice*, *16*(12), 1509–1518.

Bullo, F., & Lewis, A. D. (2004). *Geometric Control of Mechanical Systems: Modeling, Analysis, and Design for Simple Mechanical Control Systems, Vol. 49*. Springer Science & Business Media.

Burri, M., Nikolic, J., Gohl, P., Schneider, T., Rehder, J., Omari, S., et al. (2016). The EuRoC micro aerial vehicle datasets. *International Journal of Robotics Research*, *35*(10), 1157–1163.

Buşoniu, L., Varma, V. S., Lohéac, J., Codrean, A., Ştefan, O., Morărescu, I.-C., et al. (2020). Learning control for transmission and navigation with a mobile robot under unknown communication rates. *Control Engineering Practice*, *100*, Article 104460.

Chebly, A., Talj, R., & Charara, A. (2019). Coupled longitudinal/lateral controllers for autonomous vehicles navigation, with experimental validation. *Control Engineering Practice*, *88*, 79–96.

Choukroun, D., Bar-Itzhack, I. Y., & Oshman, Y. (2006). Novel quaternion kalman filter. *IEEE Transactions on Aerospace and Electronic Systems*, *42*(1), 174–190.

Davari, N., & Gholami, A. (2016). An asynchronous adaptive direct kalman filter algorithm to improve underwater navigation system performance. *IEEE Sensors Journal*, *17*(4), 1061–1068.

Deng, H., Krstic, M., & Williams, R. J. (2001). Stabilization of stochastic nonlinear systems driven by noise of unknown covariance. *IEEE Transactions on Automatic Control*, *46*(8), 1237–1253.

Hashim, H. A. (2020). Systematic convergence of nonlinear stochastic estimators on the special orthogonal group SO(3). *International Journal of Robust and Nonlinear Control*, *30*(10), 3848–3870.

Hashim, H. A. (2021). A geometric nonlinear stochastic filter for simultaneous localization and mapping. *Aerospace Science and Technology*, *111*, Article 106569. http://dx.doi.org/10.1016/j.ast.2021.106569.

Hashim, H. A. (2021). Gps-denied navigation: Attitude, position, linear velocity, and gravity estimation with nonlinear stochastic observer. In *2021 American Control Conference (ACC)* (pp. 1146–1151). IEEE.

Hashim, H. A., Brown, L. J., & McIsaac, K. (2019). Nonlinear pose filters on the special euclidean group SE(3) with guaranteed transient and steady-state performance. *IEEE Transactions on Systems, Man, and Cybernetics: Systems*, *PP*(PP), 1–14. http://dx.doi.org/10.1109/TSMC.2019.2920114.

Hashim, H. A., & Eltoukhy, A. E. E. (2020). Landmark and imu data fusion: Systematic convergence geometric nonlinear observer for slam and velocity bias. *IEEE Transactions on Intelligent Transportation Systems*, *PP*(PP), 1–10. http://dx.doi.org/10.1109/TITS.2020.3035550.

Hashim, H. A., & Lewis, F. L. (2020). Nonlinear stochastic estimators on the special euclidean group SE(3) using uncertain imu and vision measurements. *IEEE Transactions on Systems, Man, and Cybernetics: Systems*, *PP*(PP), 1–14. http://dx.doi.org/10.1109/TSMC.2020.2980184.

Hua, M.-D., & Allibert, G. (2018). Riccati observer design for pose, linear velocity and gravity direction estimation using landmark position and imu measurements. In *2018 IEEE Conference on Control Technology and Applications (CCTA)* (pp. 1313–1318). IEEE.

Hua, M.-D., Manerikar, N., Hamel, T., & Samson, C. (2018). Attitude, linear velocity and depth estimation of a camera observing a planar target using continuous homography and inertial data. In *2018 IEEE International Conference on Robotics and Automation (ICRA)* (pp. 1429–1435). IEEE.

Hua, M.-D., Zamani, M., Trumpf, J., Mahony, R., & Hamel, T. (2011). Observer design on the special euclidean group se (3). In *2011 50th IEEE Conference on Decision and Control and European Control Conference* (pp. 8169–8175). IEEE.

Ito, K., & Rao, K. M. (1984). *Lectures on Stochastic Processes, Vol. 24*. Tata institute of fundamental research.

Janabi-Sharifi, F., & Marey, M. (2010). A kalman-filter-based method for pose estimation in visual servoing. *IEEE Transactions on Robotics*, *26*(5), 939–947.

Jazwinski, A. H. (2007). *Stochastic Processes and Filtering Theory*. Courier Corporation.

Ji, H.-B., & Xi, H.-S. (2006). Adaptive output-feedback tracking of stochastic nonlinear systems. *IEEE Transactions on Automatic Control*, *51*(2), 355–360.

Lee, T. (2012). Exponential stability of an attitude tracking control system on so (3) for large-angle rotational maneuvers. *Systems & Control Letters*, *61*(1), 231–237.

Leishman, R. C., & McLain, T. W. (2015). Multiplicative extended kalman filter for relative rotorcraft navigation. *Journal of Aerospace Information Systems*, *12*(12), 728–744.

Mahony, R., Hamel, T., & Pflimlin, J.-M. (2008). Nonlinear complementary filters on the special orthogonal group. *IEEE Transactions on Automatic Control*, *53*(5), 1203–1218.

Markley, F. L. (2003). Attitude error representations for kalman filtering. *Journal of Guidance, Control, and Dynamics*, *26*(2), 311–317.

Shi, J., et al. (1994). Good features to track. In *1994 Proceedings of IEEE Conference on Computer Vision and Pattern Recognition* (pp. 593–600). IEEE.

Vasconcelos, J. F., Cunha, R., Silvestre, C., & Oliveira, P. (2010). A nonlinear position and attitude observer on se (3) using landmark measurements. *Systems & Control Letters*, *59*(3–4), 155–166.

Wei, T., Li, X., & Stojanovic, V. (2021). Input-to-state stability of impulsive reaction–diffusion neural networks with infinite distributed delays. *Nonlinear Dynamics*, *103*(2), 1733–1755.

Woodman, O. J. (2007). *An Introduction to Inertial Navigation: Tech. Rep.*, University of Cambridge, Computer Laboratory.

Zamani, M., Trumpf, J., & Mahony, R. (2013). Minimum-energy filtering for attitude estimation. *IEEE Transactions on Automatic Control*, *58*(11), 2917–2921.

Zhang, P., Gu, J., Milios, E. E., & Huynh, P. (2005). Navigation with imu/gps/digital compass with unscented kalman filter. In *IEEE International Conference Mechatronics and Automation, Vol. 3* (pp. 1497–1502). IEEE, 2005.

Zhao, B., Skjetne, R., Blanke, M., & Dukan, F. (2014). Particle filter for fault diagnosis and robust navigation of underwater robot. *IEEE Transactions on Control Systems Technology*, *22*(6), 2399–2407.